Phys. Lett. B 864 (2025) 139423

Contents lists available at ScienceDirect

Physics Letters B

journal homepage: www.elsevier.com/locate/physletb

Letter

# The charge and magnetic radii of the nucleons from the generalized parton distributions

The MMGPDs [1] Collaboration

Muhammad Goharipour [a,b,*], Fatemeh Irani [a], Hadi Hashamipour [c], K. Azizi [a,b,d]

[a] Department of Physics, University of Tehran, North Karegar Avenue, Tehran 14395-547, Iran
[b] School of Particles and Accelerators, Institute for Research in Fundamental Sciences (IPM), P. O. Box 19395-5531, Tehran, Iran
[c] Istituto Nazionale di Fisica Nucleare, Gruppo collegato di Cosenza, I-87036 Arcavacata di Rende, Cosenza, Italy
[d] Department of Physics, Dogus University, Dudullu-Ümraniye, 34775 Istanbul, Türkiye

ARTICLE INFO

Editor: A. Ringwald

ABSTRACT

The proton-radius puzzle refers to the discrepancy observed in measurements of the proton's charge radius when using different methods. This inconsistency has prompted extensive research and debate within the physics community, as it challenges the understanding of quantum electrodynamics and the fundamental properties of protons. In the present study, we determine the charge and magnetic radii of the proton and neutron through a global analysis of the generalized parton distributions (GPDs) at zero skewness. We emphasize the importance of a simultaneous analysis of all available experimental data related to nucleon radii, rather than relying on individual experiments, specific observables, or limited kinematic regions. This comprehensive approach ensures robust and consistent results, avoiding values that are either too small or too large. Our analysis yields the following results: $r_{pE} = 0.8558 \pm 0.0135$ fm, $r_{pM} = 0.8268 \pm 0.0533$ fm, $\langle r_{nE}^2 \rangle = -0.1181 \pm 0.0270$ fm$^2$, and $r_{nM} = 0.8367 \pm 0.0845$ fm.

***Introduction*** Understanding the internal structure of nucleons, encompassing protons and neutrons, remains a fundamental pursuit in modern nuclear and particle physics. Central to this investigation are the charge and magnetic radii of the nucleons, critical parameters that reveal the spatial distribution of their electric charge and magnetic moment [1]. These properties not only illuminate the dynamics within atomic nuclei but also serve as crucial benchmarks for testing theoretical models, particularly quantum electrodynamics (QED) and quantum chromodynamics (QCD).

The charge radius of a nucleon defines the spatial extent over which its electric charge is distributed, while the magnetic radius characterizes the distribution of its magnetic moment. Precise measurements of these radii serve as stringent tests for theories such as chiral effective field theory [2] and lattice QCD calculations [3]. Electromagnetic scattering experiments [4,5], utilizing high-energy electron beams, have traditionally been employed to determine these radii by measuring the cross section of the elastic scattering of electrons off nucleons in terms of the negative of the square of the four-momentum transfer $Q^2 = -t$. In fact, it is now well established that the scattering experiments access to the charge and magnetic radii of the nucleons through the slope of the electromagnetic form factors (FFs) at $Q^2 = 0$. In parallel, spectroscopic techniques, such as hydrogen (H) or muonic hydrogen ($\mu$H) spectroscopy, provide an alternative avenue for probing nucleon structure [6,7]. These methods involve studying the energy levels and transitions within exotic atoms, while scattering experiments offer direct access to the nucleon's radii via electromagnetic interactions, spectroscopy provides a unique perspective through atomic energy level measurements.

In 2010, the CREMA collaboration performed a challenging muonic hydrogen spectroscopy experiment, an improvement of the hydrogen spectroscopy method wherein the electron is replaced by a muon, and reported a value of the proton charge radius ($r_p$) which was in disagreement with previous determinations from both ordinary hydrogen spectroscopy and elastic scattering experiments [6]. This finding, which was referred to as the "proton-radius puzzle", has been a critical subject to investigate in both experimental and theoretical particle physics for more than a decade [8–13]. However, two recent measurements from

* Corresponding author at: School of Particles and Accelerators, Institute for Research in Fundamental Sciences (IPM), P. O. Box 19395-5531, Tehran, Iran.
*E-mail addresses:* muhammad.goharipour@ipm.ir (M. Goharipour), f.irani@ut.ac.ir (F. Irani), hadi.hashamipour@lnf.infn.it (H. Hashamipour), kazem.azizi@ut.ac.ir (K. Azizi).

[1] Modern Multipurpose GPDs.

https://doi.org/10.1016/j.physletb.2025.139423
Received 27 January 2025; Received in revised form 14 March 2025; Accepted 24 March 2025
Available online 25 March 2025

both hydrogen spectroscopy [14] and electron-proton ($ep$) elastic scattering from PRad experiment [15] at Jefferson Laboratory (JLab) are in agreement with the muonic hydrogen spectroscopy results which lead to smaller values for $r_p$ of about 0.83 fm. Note that the PRad result is the first measurement of $r_p$ obtained from elastic scattering experiments that is in agreement with the muonic hydrogen spectroscopy results. Actually, the results from previous elastic scattering experiments are larger than the PRad result even up to 5 standard deviations. The reason has been attributed to the fact that the PRad experiment covers the measurements of the $ep$ elastic scattering cross section (and hence the electric FF) at very small values of $Q^2$. Nevertheless, a recent study [16] shows that analyzing PRad data besides other data belonging to larger values of $Q^2$ leads to a larger value of $r_p$ which is again in disagreement with the muonic hydrogen spectroscopy results.

The precise measurements of the nucleon's charge and magnetic radii are also important for the global analysis of the generalized parton distributions (GPDs) at zero longitudinal momentum transfer $\xi$, known as skewness, since they can provide crucial constraints on GPDs at very small $Q^2$ [17–19]. Representing correlations between the longitudinal momentum and the transverse position and of partons inside the nucleon, GPDs are nonperturbative entities which can provide a 3D description of nucleons [20–29]. So, in this context, they have a significant advantage compared with ordinary parton distribution functions (PDFs) that describe only the longitudinal momentum distribution of partons inside hadrons. This is why the GPDs topic has received a lot of attention in recent years [30–49]. Note that this list is not exhaustive, as it is nearly impossible to provide a fully comprehensive compilation of all relevant GPD-related studies within the scope of this paper. At zero skewness, GPDs can be determined from a simultaneous analysis of the experimental data from different kinds of elastic scattering processes including the elastic lepton-nucleon scattering [19], elastic (anti)neutrino-nucleon scattering [34], and wide-angle Compton scattering (WACS) [18]. An important property of GPDs is that their first moments are related to different types of nucleon FFs and hence the nucleon's radii. Therefore, it is of significant interest to see how GPDs determined from a simultaneous analysis of the electromagnetic FFs (or elastic scattering cross sections) predict the charge and magnetic radii of the nucleons. Are the obtained values for radii in agreement with PRad and muonic hydrogen spectroscopy results?

It is worth noting that the determination of GPDs at zero skewness through the analysis of electromagnetic FFs and their impact on nucleon radii has been performed before, for example, in Refs. [31,32]. However, such analyses are based on fewer experimental data points, limited to elastic electron-nucleon scattering, and employed simpler ansatz. The present study utilizes a wide range of experimental data, including both elastic electron-nucleon scattering and quasielastic antineutrino-nucleon scattering. Our analysis is based on a comprehensive data set from the more recent YAHL18 analysis [50] and incorporates new GMp12 data from JLab [51] as well as neutrino data from the PRad experiment [15].

In the present study, we first perform a standard $\chi^2$ analysis of a wide range of the elastic electron-nucleon scattering as well as the antineutrino-nucleon scattering experimental data and determine simultaneously the unpolarized valence GPDs $H_v^q$ and $E_v^q$ with their uncertainties. Then, using the extracted GPDs, we calculate the charge and magnetic radii of both proton and neutron and compare them with the corresponding ones obtained from various elastic scattering experiments and hydrogen spectroscopy.

***Formalism*** As mentioned before, the charge and magnetic radii of the nucleons are directly related to the electric and magnetic FFs, $G_E^j(Q^2)$ and $G_M^j(Q^2)$, which encode the internal charge and magnetization distributions. Here $j = p, n$ where $p$ and $n$ denote the proton and neutron, respectively. To be more precise, the mean squared of the charge and magnetic radii of the nucleons, $r_{jE}$ and $r_{jM}$, can be obtained from the slope of the electromagnetic FFs at $t = 0$ as follows [17]

$$\left\langle r_{jE}^2 \right\rangle = 6\frac{\mathrm{d}G_E^j}{\mathrm{d}t}\bigg|_{t=0}, \qquad \left\langle r_{jM}^2 \right\rangle = \frac{6}{\mu_j}\frac{\mathrm{d}G_M^j}{\mathrm{d}t}\bigg|_{t=0}, \tag{1}$$

where $\mu_j$ is the magnetic moment of the nucleon. The electromagnetic FFs $G_E$ and $G_M$ which are commonly called Sachs FFs are expressed in terms of the Dirac and Pauli FFs of the nucleon, $F_1$ and $F_2$,

$$\begin{aligned} G_M(t) &= F_1(t) + F_2(t), \\ G_E(t) &= F_1(t) + \frac{t}{4m^2}F_2(t), \end{aligned} \tag{2}$$

where $m$ is the nucleon's mass.

Experimentally, the Sachs FFs can be extracted from the measurements of the cross section of the elastic electron-nucleon scattering [50] that is often presented as the reduced cross section

$$\begin{aligned} \sigma_R &= \epsilon G_E^2(t) + \tau G_M^2(t), \\ &= G_M^2(t)[\tau + \epsilon \mathrm{RS}(t)/\mu_j^2], \end{aligned} \tag{3}$$

where $\epsilon$ and $\tau$ are the dimensionless kinematic variables and $\mathrm{RS} = (\mu G_E/G_M)^2$ is the normalized Rosenbluth slope [51]. The method that provides the separate determination of $G_E$ and $G_M$ is called the Rosenbluth separation in which the unpolarized elastic electron-nucleon scattering is considered. However, there is another method in which one can use the correlation between the polarizations of the electron and nucleon to extract Sachs FFs. Although such a method has the advantage that it is less sensitive to two-photon exchange (TPE) corrections, one can only access the ratio of Sachs FFs in this method.

Theoretically, the Dirac and Pauli FFs can be obtained from the unpolarized valence GPDs $H_v^q$ and $E_v^q$ at zero skewness ($\xi = 0$). Here $q$ denotes the up, down, and strange quarks, though we can neglect the strange contribution. Considering the proton case, we have the following sum rules [31,32]

$$\begin{aligned} F_1^p(t) &= \sum_q e_q F_1^q(t) = \sum_q e_q \int_0^1 dx\, H_v^q(x,\mu^2,t), \\ F_2^p(t) &= \sum_q e_q F_2^q(t) = \sum_q e_q \int_0^1 dx\, E_v^q(x,\mu^2,t), \end{aligned} \tag{4}$$

where $x$ represents the longitudinal momentum fraction of the nucleon carried by quark $q$ with electric charge $e_q$, and $\mu^2$ stands for the factorization scale at which the quarks are resolved. Note that the related formulas for the neutron FFs $F_1^n$ and $F_2^n$ can be obtained by assuming the isospin symmetry, i.e., $u^p = d^n, d^p = u^n$.

According to the above equations, by measuring the reduced cross section $\sigma_R$ or equivalently the electromagnetic FFs $G_E$ and $G_M$, one can determine the unpolarized valence GPDs $H_v^q$ and $E_v^q$ at zero skewness by performing a standard $\chi^2$ analysis and considering suitable parameterizations for GPDs [17–19]. On the other hand, one can calculate the nucleon's charge and magnetic radii using Eq. (1) and extracted GPDs. This approach to calculate the nucleon's radii is really of interest because GPDs are determined from a simultaneous analysis of a wide range of experimental data from the elastic electron scattering off both proton and neutron. While the experimental measurements of the nucleon's radii from elastic scattering experiments are usually based on the fit to certain data (with limited kinematic coverage) and to one kind of FFs solely. For example, in the PRad experiment [15], the valued of $r_p = 0.831$ fm has been obtained by analyzing just the electric FF data in the $t$ range of $0.0002 \lesssim -t \lesssim 0.06$ GeV$^2$. So, the values of the radii of the nucleons determined from the global analysis of GPDs can be crucial in the context of the proton-radius puzzle.

The first step to extract GPDs from the $\chi^2$ analysis of the related experimental data is to choose a suitable parametrization for them. It is now well established that the following ansatz which relates GPDs to ordinary PDFs works well [17–19,32]

$$H_v^q(x,\mu^2,t) = q_v(x,\mu^2)\exp\left[t f_v^q(x)\right],$$
$$E_v^q(x,\mu^2,t) = e_v^q(x,\mu^2)\exp\left[t g_v^q(x)\right], \quad (5)$$

where $q_v(x,\mu^2)$ represents the unpolarized valence PDF for quark flavor $q$. As in our previous analysis [19], utilizing the LHAPDF package [52], we take PDFs from the NNPDF analysis [53] at the next-to-leading order (NLO) and scale $\mu = 2$ GeV. Note that the above ansatz satisfies the requirement that GPDs are reduced to PDFs at the so-called forward limit ($t = 0$ and $\xi = 0$). Since $e_v^q(x,\mu^2)$ is not available from the analysis of the high-energy experimental data, we have to determine it from the fit to data too. To this aim, we consider the following parametrization [17–19,32]

$$e_v^q(x,\mu^2) = \kappa_q N_q x^{-\alpha_q}(1-x)^{\beta_q}(1+\gamma_q\sqrt{x}), \quad (6)$$

where $\kappa_u = 1.67$ and $\kappa_d = -2.03$ are the magnetic moments of the up and down quarks, respectively, in the units of nuclear magneton. They have been extracted from the corresponding values of the magnetic moments of proton and neutron taken from [54]. The profile functions $f_v^q(x)$ and $g_v^q(x)$ in Eq. (5) describe the damping of GPDs with respect to PDFs as the value of $t$ increases. We use the following form to parameterize them as suggested in [32]

$$\mathcal{F}(x) = \alpha'(1-x)^3\log\frac{1}{x} + B(1-x)^3 + Ax(1-x)^2. \quad (7)$$

In this way, for each quark flavor, the unknown free parameters that must be determined from the $\chi^2$ analysis of the experimental data are $\alpha$, $\beta$, $\gamma$, $\alpha'$, $A$, and $B$. Note that the experimental error associated with each measured data point that is used in the calculation of the $\chi^2$ function is obtained by adding the systematic and statistical errors in quadrature. As in Refs. [17–19], the CERN program library MINUIT [55] is used for performing the minimization procedure and determining the optimum values of the unknown parameters. Also, the standard Hessian approach [56] with $\Delta\chi^2 = 1$ is used to calculate uncertainties. Another point that should be mentioned is that we impose the condition $g_v^q(x) < f_v^q(x)$ in the main body of the fit program to satisfy the positivity property of GPDs in a wide range of the $x$ values. Moreover, in order to determine the optimum values of the unknown parameters, we adopt the parametrization scan procedure in which the final parametrization of each distribution is obtained systematically. See Refs. [17–19] to get more information about our phenomenological framework.

Now it is time to discuss the experimental data sets that we use in our analysis of GPDs. The main body of the experimental data that we consider in the present study is as our recent analysis [19] where we have investigated the impact of JLab data at high values of $Q^2$ on the extracted GPDs at zero skewness. These data include the world $R^p = \mu_p G_E^p/G_M^p$ polarization, $G_E^n$, and $G_M^n/\mu_n G_D$ measurements from the YAHL18 analysis [50], the data of $G_E^p$ from AMT07 [57] and Mainz [58] and the measurements of the reduced cross-section $\sigma_R$ from JLab experiment [51], namely GMp12. Overall, these data cover the $-t$ range from 0.007 to 15.76 GeV$^2$. As mentioned before, in the present study we also add the PRad data [15] which cover the $-t$ range from 0.00022 to 0.05819 GeV$^2$ (note that we use both 1.1 GeV and 2.2 GeV data). The total number of data with and without PRad data is 348 and 277, respectively.

***Analysis and Results*** In the following, we first determine the unpolarized valence GPDs $H_v^q$ and $E_v^q$ at zero skewness by performing three analyses. In the first analysis, we consider all data sets described before except PRad data which leads to a set of GPDs without any from PRad data. We call this analysis "Base Fit". The second analysis is performed by including also the PRad data in the analysis. In this way we can investigate the impact of these data on the final results separately. We call this analysis "PRad". In the third analysis, we repeat the second analysis by removing the Mainz data considering the fact that there is a significant tension between them and AMT07 world data [18,50]. This analysis is called "PRad_NoMainz".

Table 1 presents the values of $\chi^2$ for the three analyses described above. In the first column, we have listed the data sets with their corresponding observables and references. For each dataset, we have presented the values of $\chi^2$ per number of data points, $\chi^2/N_{\text{pts.}}$, obtained from the Base Fit, PRad, and PRad_NoMainz analyses in the second, third, and fourth columns, respectively. In the last row of the table, we have presented the values of total $\chi^2$ divided by the number of degrees of freedom, $\chi^2$/d.o.f., for each analysis. As can be seen, the PRad data are in good consistency with other elastic scattering measurements so that including them in the analysis does not change significantly the $\chi^2$ of the other data sets. Moreover, removing the Mainz data from the analysis leads to a significant decrease in the value of total $\chi^2$ and hence $\chi^2$/d.o.f.

**Table 1**
The values of $\chi^2$ per number of data points obtained from the Base Fit, PRad, and PRad_NoMainz analyses. The values of total $\chi^2$ divided by the number of degrees of freedom have been presented in the last row. See text for more details.

| Observable | $\chi^2/N_{\text{pts.}}$ | | |
|---|---|---|---|
| | Base Fit | PRad | PRad_NoMainz |
| Mainz $G_E^p$ [58] | 275.1/77 | 281.6/77 | – |
| AMT07 $G_E^p/G_D$ [57] | 37.2/47 | 37.1/47 | 40.3/47 |
| AMT07 $R^p$ [50] | 115.6/69 | 115.7/69 | 111.7/69 |
| AMT07 $G_E^n$ [50] | 30.1/38 | 27.1/38 | 25.2/38 |
| AMT07 $G_M^n/\mu_n G_D$ [50] | 32.5/33 | 34.4/33 | 33.8/33 |
| GMp12 $\sigma_R$ [51] | 16.2/13 | 18.4/13 | 13.7/13 |
| PRad $\sigma_R$ [15] 1.1 GeV | – | 10.5/33 | 10.2/33 |
| PRad $\sigma_R$ [15] 2.2 GeV | – | 45.1/38 | 44.2/38 |
| Total $\chi^2$/d.o.f. | 506.7/262 | 569.9/333 | 279.1/256 |

**Table 2**
The optimum values of the parameters of the profile functions (7), and distributions $e_v^q(x)$ of Eq. (6) obtained from three analyses described in the text.

| Distribution | Parameter | Base Fit | PRad | PRad_NoMainz |
|---|---|---|---|---|
| $f_v^u(x)$ | $\alpha'$ | $0.745 \pm 0.016$ | $0.728 \pm 0.015$ | $0.704 \pm 0.019$ |
| | $A$ | $1.017 \pm 0.053$ | $0.992 \pm 0.050$ | $0.939 \pm 0.049$ |
| | $B$ | $0.772 \pm 0.049$ | $0.819 \pm 0.046$ | $0.884 \pm 0.051$ |
| $f_v^d(x)$ | $\alpha'$ | $0.405 \pm 0.051$ | $0.380 \pm 0.045$ | $0.350 \pm 0.053$ |
| | $A$ | $1.273 \pm 0.402$ | $1.561 \pm 0.394$ | $1.559 \pm 0.490$ |
| | $B$ | $1.590 \pm 0.211$ | $1.627 \pm 0.190$ | $1.683 \pm 0.226$ |
| $g_v^u(x)$ | $\alpha'$ | $\alpha'_{f_v^u}$ | $\alpha'_{f_v^u}$ | $\alpha'_{f_v^u}$ |
| | $A$ | $0.163 \pm 0.140$ | $0.318 \pm 0.153$ | $0.318 \pm 0.143$ |
| | $B$ | 0.000 | 0.000 | 0.000 |
| $g_v^d(x)$ | $\alpha'$ | $0.606 \pm 0.258$ | $0.617 \pm 0.158$ | $0.682 \pm 0.274$ |
| | $A$ | $1.429 \pm 1.514$ | $1.718 \pm 0.980$ | $1.722 \pm 1.135$ |
| | $B$ | 0.000 | 0.000 | 0.000 |
| $e_v^u(x)$ | $\alpha$ | $0.699 \pm 0.047$ | $0.702 \pm 0.054$ | $0.679 \pm 0.033$ |
| | $\beta$ | $8.178 \pm 0.484$ | $7.422 \pm 0.600$ | $7.530 \pm 0.587$ |
| | $\gamma$ | $6.555 \pm 3.107$ | $4.371 \pm 3.418$ | $2.868 \pm 1.515$ |
| $e_v^d(x)$ | $\alpha$ | $0.837 \pm 0.059$ | $0.816 \pm 0.040$ | $0.813 \pm 0.062$ |
| | $\beta$ | $7.189 \pm 5.065$ | $6.840 \pm 2.975$ | $6.389 \pm 3.336$ |
| | $\gamma$ | $15.626 \pm 9.326$ | $12.531 \pm 5.959$ | $15.856 \pm 11.205$ |

Following the parametrization scan procedure outlined in [17,18,34], we identify a set of GPDs characterized by $\alpha'_{g_v^u} = \alpha'_{f_v^u}$, $B_{g_v^u} = 0$, and $B_{g_v^d} = 0$. Notably, releasing these parameters does not result in a reduction of the $\chi^2$ value or any improvement in the quality of the fit. The remaining parameters are determined through a standard fit to the data. Table 2 presents the optimal values of these parameters obtained from the three analyses described above. As evident from the results, the inclusion of the PRad data in the analysis considerably reduces the uncertainties of the parameters, particularly of GPD $E_v^d$. Additionally, the central values of some parameters exhibit notable changes. On the other hand, removing the Mainz data from the analysis does not substantially alter the final results, particularly for the GPDs $H_v^q$. However,

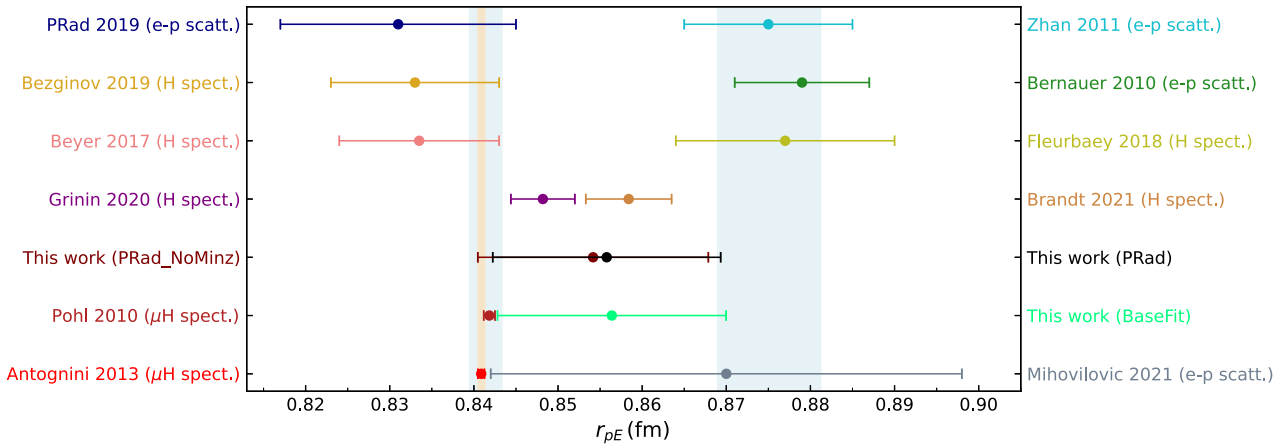


**Fig. 1.** A comparison between the results obtained for the proton charge radius $r_{pE}$ from three analyses performed in this study and the corresponding values obtained from various experiments. See text to get more information.

**Table 3**
The results obtained for the proton and neutron charge and magnetic radii from three GPD analyses performed in the present study.

| Observable | Base Fit | PRad | PRad_NoMainz |
|---|---|---|---|
| $r_{pE}$ | $0.8564 \pm 0.0136$ | $0.8558 \pm 0.0135$ | $0.8542 \pm 0.0137$ |
| $r_{pM}$ | $0.8242 \pm 0.0596$ | $0.8268 \pm 0.0533$ | $0.8243 \pm 0.0605$ |
| $< r^2_{nE} >$ | $-0.1132 \pm 0.0272$ | $-0.1181 \pm 0.0270$ | $-0.1244 \pm 0.0274$ |
| $r_{nM}$ | $0.8330 \pm 0.1136$ | $0.8367 \pm 0.0845$ | $0.8426 \pm 0.1230$ |

some variations are observed in the forward limits $e^q_v(x)$ of the GPDs $E^q_v$.

After determining the unpolarized valence GPDs $H^q_v$ and $E^q_v$ at zero skewness, now we can calculate the corresponding electromagnetic FFs and hence the charge and magnetic radii of the nucleons using Eq. (1). The results obtained for the proton and neutron charge and magnetic radii from three GPD analyses performed in the present study have been summarized in Table 3. Note that the uncertainties have been calculated by considering also the uncertainties from the NNPDF PDFs (in fact, they have significant contributions).

According to the results obtained, either including the PRad data or removing the Mainz data, which both cover the small $-t$ region, does not lead to a significant change in the values of $r_{pE}$ and $r_{pM}$. This clearly shows that the global analysis of GPDs including a wide range of experimental data (covering a wide range of $-t$) leads to averaged values for the radii of the nucleons comparing with the case where just the data from a certain experiment or a specific observable are analyzed. For example, analyzing the PRad data solely (covering very small $-t$ region) results in a small value for $r_{pE}$ [15], while analyzing them besides other data (whether with small or large values of $-t$) leads to different values (larger) for $r_{pE}$ [16]. That's exactly why including the PRad data or removing the Mainz data leads to a considerable change in the values of $< r^2_{nE} >$ and $r_{nM}$. In fact, since in the case of neutron we have fewer data, adding or removing some data points can affect the final results. As can be seen, both $< r^2_{nE} >$ and $r_{nM}$ have increased (in magnitude) by adding the PRad data to the analysis. They have even increased more by removing the Mainz data from the analysis. In a quantitative view, e.g., the central value of $< r^2_{nE} >$ has changed about 10 percent from the Base fit analysis to the PRad_NoMainz analysis or the magnitude of the uncertainty of $r_{nM}$ has decreased about 34 percent from the Base fit analysis to the PRad analysis. Another point that should be noted is that the large uncertainties of $r_{nM}$ come from the large uncertainties of GPDs $E^q_v$ of the neutron which have greater contributions in $G^n_M$ rather than $G^n_E$ due to the greater contribution of $F_2$ in $G^n_M$, especially at small values of $-t$. Overall, a significant part of uncertainties comes from the PDF uncertainties. For example, by excluding the PDF uncertainties, the error of $r_{pE}$ is decreased from 0.0135 to 0.0031 (the reductions are more significant for the charge radii compared to the magnetic radii). Note also that the PRad data leads to a significant reduction in the uncertainty of $r_{nM}$ and its uncertainty becomes again very large after removing the Mainz data of $G^p_E$. Therefore, one should pay special attention to the fact that how adding or removing the data belonging to the proton can affect the results obtained for the neutron (both in value and uncertainty). So, it seems that analyzing all experimental data related to the radii of the nucleons simultaneously would be preferable.

Fig. 1 shows a comparison between the results obtained for the proton charge radius $r_{pE}$ from three analyses performed here and the corresponding values obtained from various experiments. The right band and the left wider band belong to the CODATA 2014 [59] and CODATA 2018 [60], respectively, while the left narrow band has been taken from PDG 2024 [54]. For the scattering experiments, we have presented the results of Refs. [15,61–63]. The ordinary hydrogen spectroscopy results have been taken from Refs. [7,14,64–66], while for the muonic hydrogen spectroscopy we have used the results of Refs. [6,67]. As can be seen, there is a large gap between some experiments referred to as the proton-radius puzzle. Except for the PRad experiment, other scattering experiments resulted in a large value for $r_{pE}$ (note that, as discussed before, if PRad data are analyzed besides other scattering data, $r_{pE}$ would not be as small as the PRad result). Although the older hydrogen spectroscopy results comprise both small and large $r_{pE}$ regions, two recent measurements [7,66] lie inside the gap. In contrast, the muonic hydrogen spectroscopy leads just to small values of $r_{pE}$. An interesting thing is that our results which have been obtained from the global analyses of GPDs are placed in the middle of the gap. As if the simultaneous analysis of all data leads to an average value for $r_{pE}$. Anyway, our results are in better consistency with recent hydrogen spectroscopy results.

In order to cross check the results obtained and the conclusion reached, we perform a new analysis by including only the PRad data in the analysis and removing other data sets. In this case, the total number of data points included in the analysis would be 71. Such an analysis should basically lead to the same result as PRad experiment for the proton charge radius $r_{pE}$. Since the PRad data cover only the very small $-t$ region, there is no need to consider parameters $A$ and $B$ in profile functions (they control the medium and large $-t$ regions). On the other hand, since PRad data can not provide enough constraints on parameters $\alpha'$, we consider them to be equal (note that releasing others does not lead to a significant decrease in the value of $\chi^2$ and hence does not improve the quality of the fit). For the forward PDF $e^q_v$, we use the distributions obtained from the PRad analysis. The value of total $\chi^2$ divided by the number of degrees of freedom, $\chi^2$/d.o.f., obtained for this analysis is 0.35 which clearly indicates the good quality of the fit. By calculating the $r_{pE}$ using the GPDs extracted, one ob-

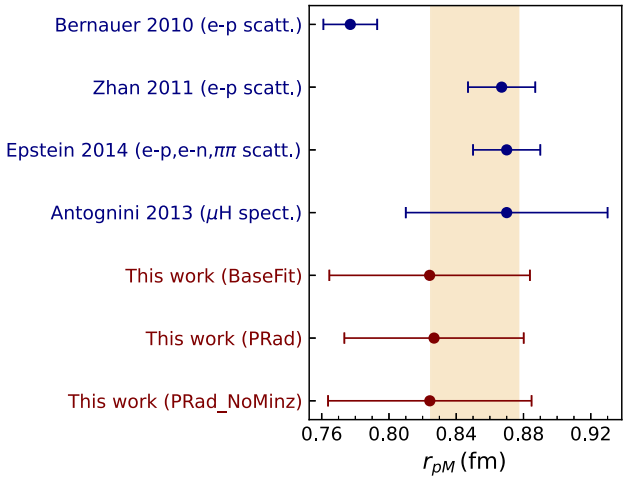


**Fig. 2.** Same as Fig. 1 but for the proton magnetic radius $r_{pM}$.

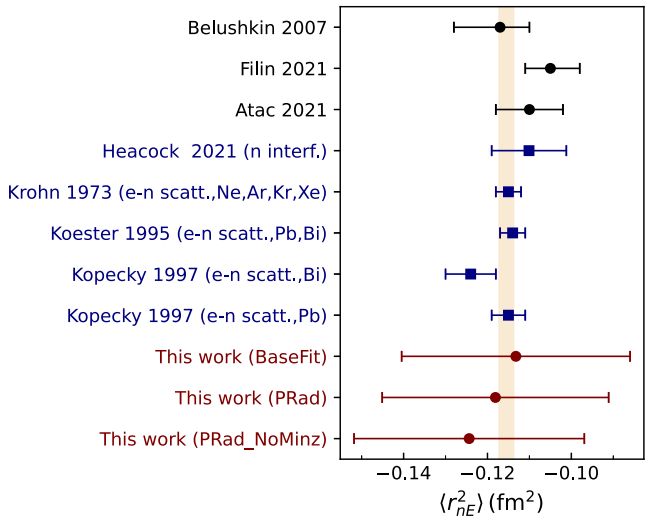


**Fig. 3.** A comparison between the results obtained for $< r^2_{nE} >$ from three analyses performed in this study and the corresponding values obtained from various experiments analyses. See text to get more information.

tains $r_{pE} = 0.834 \pm 0.008$ fm. This value is in complete agreement with the PRad experiment $r_{pE} = 0.831 \pm 0.014$ fm. This result clearly establishes that considering the medium and large $-t$ data points as well as other observables in a global analysis of GPDs really changes the extracted value of the $r_{pE}$. As one includes more data in the analysis from various observables covering wider range of $-t$, the extracted $r_{pE}$ becomes more process (or experiment) independent and closer to a unique value.

To be more precise, in our method to determine the nucleon's radii, both large and small $-t$ data are expected to affect the final results. Please note that the nucleon's radii are also proportional to the profile functions through the derivation of GPDs. This means that even at $t = 0$ limit, the $x$-dependence of the profile functions play a crucial role in the values obtained for radii. In other words, the parameters $A$ and $B$ in Eq. (7) which are controlled with the medium and large $-t$ data would be also important. While data belonging to the small values of $-t$ (such as PRad data) are associated with the parameters $\alpha'$ (note also that the large $-t$ region is corresponding to the large $x$ region and vice versa). This is exactly the reason for the importance of both small and large $-t$ data when one determines the nucleus's radii through the analysis of GPDs. Actually, since the forward limit $e^q_v$ and the profile functions $f^q_v(x)$ and $g^q_v(x)$ are obtained from whole $-t$ regions, the medium and large $-t$ regions are also important and can affect the value of radii. Mathematically, this means that one should first obtain the whole $-t$ dependency of FFs and then calculate their derivations at $t = 0$.

Fig. 2 shows the same comparison as Fig. 1 but for the proton magnetic radius $r_{pM}$. In this case, there is less information from the experiment compared with the measurements of $r_{pE}$. We have presented three results from the scattering experiments [61,62,68] and only one result from the muonic hydrogen spectroscopy [67]. Note that the value presented by Epstein et al. has been extracted in a model independent way from the electron-proton scattering data in addition to the electron-neutron scattering and $\pi\pi \to N\bar{N}$ data. The band shows the corresponding value taken from PDG 2024 [54]. As can be seen, in this case, the results of different experiments are in better consistency with each other compared with $r_{pE}$, especially considering the uncertainties. For example, in Fig. 1 there is a large gap between the results of Zhan 2011 [62] and Antognini 2013 [67] for $r_{pE}$ referring to the proton radius puzzle, while the corresponding values for $r_{pM}$ from these two experiments are in complete agreement. An interesting thing is that our results are almost the average of other data like the case of $r_{pE}$.

The results obtained for $< r^2_{nE} >$ have been presented in Fig. 3 and compared with the available experimental measurements [69–72] (square symbols) and the corresponding values obtained from various analyses including the dispersion analysis of the nucleon electromagnetic FFs data [73], chiral effective field theory [74], and the extraction of the neutron electric FF from the nucleon-to-delta ($N \to \Delta$) quadrupole transitions [75]. As before, the band shows the value taken from PDG 2024. The experimental measurements mostly belong to the electron-neutron scattering experiments through the scattering off different nuclei. However, there is a measurement [69] from an unusual method called Pendellösung interferometry where the momentum dependence of the structure factors enabled the researchers to measure the charge radius of the neutron. As can be seen, all results are in good consistency with each other. As mentioned before, the large uncertainties in our results come from our poor knowledge of the neutron GPDs due to the lack of data in this case (note that the uncertainties include also the PDFs uncertainties which are relatively large, especially in the case of NNPDF). Actually, it is vital to measure the neutron electromagnetic FFs precisely to put strong constraints on the forward limit of the down quark GPD $E^d_v$ and its profile function to reduce the uncertainty of the charge and magnetic radii of the neutron. Note that the radii are related also to the profile functions through the derivation of the exponential in ansatz (5).

Fig. 4 shows the same comparison as Fig. 3 but for the neutron magnetic radius $r_{nM}$. In this case, there is only one measurement by Epstein et al. from the scattering experiments. In addition to the results of Belushkin 2007 [73] and Filin 2021 [74] described before, here we have also presented the results of two other analyses, namely, Borah 2020 [76] and Lin 2022 [77]. The former has been obtained from a global fit to electron scattering data and precise charge radius measurements, while the latter has been obtained from a combined analysis of the electromagnetic FFs of the nucleon in the space- and timelike regions using dispersion theory. According to this figure, except for Borah 2020, all results are in very good agreement with each other and also the corresponding value taken from PDG 2024 (the band). Note that among the results obtained from the present study, the analysis called PRad that contains all experimental data sets (including the PRad and Mainz data) has a smaller uncertainty. This clearly indicates that inducing more precise data, especially the neutron data, in the analysis of GPDs can significantly reduce the large uncertainties observed in Figs. 3 and 4. Therefore, ongoing and upcoming experiments such as the MUSE experiment at PSI, the COMPASS++/AMBER experiment at CERN, the PRad-II experiment at JLab, and future electron scattering experiments at Mainz, and the ULQ$^2$ experiment at Tohoku University can play a crucial role in this regard. See Refs. [1,4] to get more information. The proton charge radius can even be measured through dimuon photoproduction off a proton target [78].

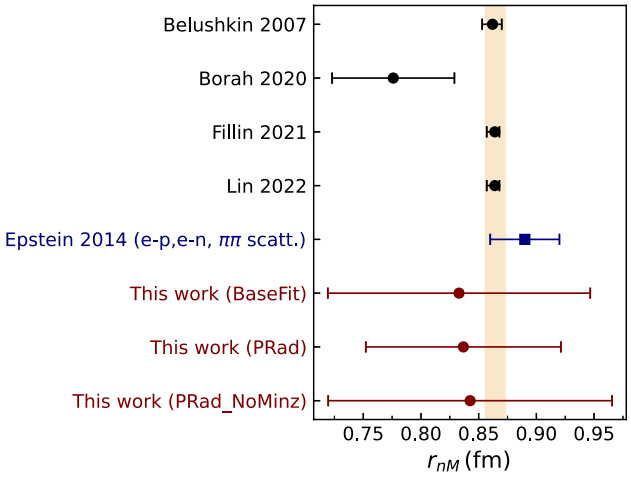


**Fig. 4.** Same as Fig. 3 but for the neutron magnetic radius $r_{nM}$.

***Conclusions*** In this study, we determined the charge and magnetic radii of the proton and neutron through a global analysis of GPDs at zero skewness for the first time. To this aim, we first extracted the unpolarized valence GPDs $H_v^q$ and $E_v^q$ with their uncertainties from a $\chi^2$ analysis of a wide range of the experimental data of the nucleons electromagnetic FFs and the elastic electron-proton reduced cross section. Then, considering the fact that the nucleon's radii are the slope of the electromagnetic FFs at $Q^2 = 0$, we calculated the proton and neutron charge and magnetic radii. The results related to the analysis that contains all experimental data sets, namely PRad, are as follows:

$$\begin{aligned} r_{pE} &= 0.8558 \pm 0.0135 \text{ fm}, \\ r_{pM} &= 0.8268 \pm 0.0533 \text{ fm}, \\ \langle r_{nE}^2 \rangle &= -0.1181 \pm 0.0270 \text{ fm}^2, \\ r_{nM} &= 0.8367 \pm 0.0845 \text{ fm}. \end{aligned} \tag{8}$$

It should be noted that the uncertainties include also the PDFs uncertainties which are relatively large. Overall, the neutron radii have larger uncertainties than the corresponding values for the proton due to the lack of information about the neutron. In this way, the ongoing and upcoming experiments [1,4] will play definitely a crucial role to shed light on this issue. For instance, it has been demonstrated now that the two-photon exclusive production of lepton pairs at the Electron-Ion Collider can provide a unique opportunity to measure the proton's elastic electromagnetic FFs and, consequently, the nucleon's radii [79].

In the context of the proton-radius puzzle, our results are placed in the middle of the gap between various experimental measurements obtained from the scattering experiments and hydrogen spectroscopy. This means that the simultaneous analysis of all data leads to an average value for $r_{pE}$ and also $r_{pM}$ extracted so far. In the case of $r_{pE}$, our results are in better consistency with recent ordinary hydrogen spectroscopy result [7,66]. For the neutron, the radii obtained from our analyses are in good consistency with the results of other experiments and analyses as well as the PDG 2024 [54].

As an important result, we showed that the global analysis of GPDs considering a wide range of the experimental data (covering a wide range of $Q^2$) ensures robust and consistent results for the radii of the nucleons, avoiding values that are either too small or too large, while analyzing the data from just a certain experiment or a specific observable leads to different results. We indicated that including or removing data belonging to the proton can affect the results obtained for the neutron (both in value and uncertainty). We emphasize the importance of a simultaneous analysis of all available experimental data related to nucleon radii, rather than relying on individual experiments, specific observables, or limited kinematic regions. Actually, this method has an advantage that it can take into account the possible correlations between the $G_E$ and $G_M$ data of the proton as well as those between the proton and neutron data.

## Declaration of competing interest

We declare that there is no conflict of interests regarding this manuscript.

## Acknowledgements

We thank Weizhi Xiong and Ashot Gasparian for providing us with the PRad data. M. Goharipour is thankful to the School of Particles and Accelerators, Institute for Research in Fundamental Sciences (IPM), for financial support provided for this research. F. Irani and K. Azizi are thankful to Iran National Science Foundation (INSF) for financial support provided for this research under grant No. 4033039.

## Data availability

The data supporting this study's findings are available within the article.

## References

[1] J.P. Karr, D. Marchand, E. Voutier, The proton size, Nat. Rev. Phys. 2 (11) (2020) 601–614.
[2] F. Gil-Domínguez, J.M. Alarcón, C. Weiss, Proton charge radius extraction from muon scattering at MUSE using dispersively improved chiral effective field theory, Phys. Rev. D 108 (7) (2023) 074026, arXiv:2306.01037 [hep-ph].
[3] S. Park, et al., Nucleon Matrix Elements (NME), Precision nucleon charges and form factors using (2+1)-flavor lattice QCD, Phys. Rev. D 105 (5) (2022) 054505, arXiv:2103.05599 [hep-lat].
[4] H. Gao, M. Vanderhaeghen, The proton charge radius, Rev. Mod. Phys. 94 (1) (2022) 015002, arXiv:2105.00571 [hep-ph].
[5] W. Xiong, C. Peng, Proton electric charge radius from lepton scattering, Universe 9 (4) (2023) 182, arXiv:2302.13818 [nucl-ex].
[6] R. Pohl, A. Antognini, F. Nez, F.D. Amaro, F. Biraben, J.M.R. Cardoso, D.S. Covita, A. Dax, S. Dhawan, L.M.P. Fernandes, et al., The size of the proton, Nature 466 (2010) 213–216.
[7] A. Grinin, A. Matveev, D.C. Yost, L. Maisenbacher, V. Wirthl, R. Pohl, T.W. Hänsch, T. Udem, Two-photon frequency comb spectroscopy of atomic hydrogen, Science 370 (6520) (2020) abc7776.
[8] R. Pohl, R. Gilman, G.A. Miller, K. Pachucki, Annu. Rev. Nucl. Part. Sci. 63 (2013) 175–204, arXiv:1301.0905 [physics.atom-ph].
[9] J.C. Bernauer, R. Pohl, The proton radius problem, Sci. Am. 310 (2) (2014) 18–25.
[10] C.E. Carlson, Prog. Part. Nucl. Phys. 82 (2015) 59–77, arXiv:1502.05314 [hep-ph].
[11] R.J. Hill, Review of experimental and theoretical status of the proton radius puzzle, EPJ Web Conf. 137 (2017) 01023, arXiv:1702.01189 [hep-ph].
[12] C. Peset, A. Pineda, O. Tomalak, The proton radius (puzzle?) and its relatives, Prog. Part. Nucl. Phys. 121 (2021) 103901, arXiv:2106.00695 [hep-ph].
[13] Y.H. Lin, H.W. Hammer, U.G. Meißner, The proton magnetic radius: a new puzzle?, Sci. Bull. 69 (2024) 419–421, arXiv:2312.08694 [hep-ph].
[14] N. Bezginov, T. Valdez, M. Horbatsch, A. Marsman, A.C. Vutha, E.A. Hessels, A measurement of the atomic hydrogen Lamb shift and the proton charge radius, Science 365 (6457) (2019) 1007–1012.
[15] W. Xiong, A. Gasparian, H. Gao, D. Dutta, M. Khandaker, N. Liyanage, E. Pasyuk, C. Peng, X. Bai, L. Ye, et al., A small proton charge radius from an electron–proton scattering experiment, Nature 575 (7781) (2019) 147–150.
[16] M. Ridwan, T. Mart, Note on the electromagnetic radius of proton, Mod. Phys. Lett. A 38 (36n37) (2023) 2350157, arXiv:2308.14950 [hep-ph].
[17] H. Hashamipour, M. Goharipour, K. Azizi, S.V. Goloskokov, Determination of the generalized parton distributions through the analysis of the world electron scattering data considering two-photon exchange corrections, Phys. Rev. D 105 (5) (2022) 054002, arXiv:2111.02030 [hep-ph].
[18] H. Hashamipour, M. Goharipour, K. Azizi, S.V. Goloskokov, Generalized parton distributions at zero skewness, Phys. Rev. D 107 (9) (2023) 096005, arXiv:2211.09522 [hep-ph].
[19] M. Goharipour, et al., MMGPDs, Impact of JLab data on the determination of GPDs at zero skewness and new insights from transition form factors $N \to \Delta$, Phys. Rev. D 109 (7) (2024) 074042, arXiv:2403.19384 [hep-ph].
[20] D. Müller, D. Robaschik, B. Geyer, F.M. Dittes, J. Hořejši, Wave functions, evolution equations and evolution kernels from light ray operators of QCD, Fortschr. Phys. 42 (1994) 101–141, arXiv:hep-ph/9812448 [hep-ph].
[21] A.V. Radyushkin, Scaling limit of deeply virtual Compton scattering, Phys. Lett. B 380 (1996) 417–425, arXiv:hep-ph/9604317 [hep-ph].
[22] X.D. Ji, Deeply virtual Compton scattering, Phys. Rev. D 55 (1997) 7114–7125, arXiv:hep-ph/9609381 [hep-ph].

[23] X.D. Ji, Gauge-invariant decomposition of nucleon spin, Phys. Rev. Lett. 78 (1997) 610–613, arXiv:hep-ph/9603249 [hep-ph].

[24] M. Burkardt, Impact parameter dependent parton distributions and off forward parton distributions for zeta —> 0, Phys. Rev. D 62 (2000) 071503; erratum: Phys. Rev. D 66 (2002) 119903, arXiv:hep-ph/0005108 [hep-ph].

[25] K. Goeke, M.V. Polyakov, M. Vanderhaeghen, Hard exclusive reactions and the structure of hadrons, Prog. Part. Nucl. Phys. 47 (2001) 401–515, arXiv:hep-ph/0106012 [hep-ph].

[26] M. Diehl, Generalized parton distributions, Phys. Rep. 388 (2003) 41–277, arXiv:hep-ph/0307382 [hep-ph].

[27] A.V. Belitsky, A.V. Radyushkin, Unraveling hadron structure with generalized parton distributions, Phys. Rep. 418 (2005) 1–387, arXiv:hep-ph/0504030 [hep-ph].

[28] S. Boffi, B. Pasquini, Generalized parton distributions and the structure of the nucleon, Riv. Nuovo Cimento 30 (9) (2007) 387–448, arXiv:0711.2625 [hep-ph].

[29] M. Diehl, Introduction to GPDs and TMDs, Eur. Phys. J. A 52 (6) (2016) 149, arXiv:1512.01328 [hep-ph].

[30] K. Kumericki, S. Liuti, H. Moutarde, GPD phenomenology and DVCS fitting: entering the high-precision era, Eur. Phys. J. A 52 (6) (2016) 157, arXiv:1602.02763 [hep-ph].

[31] M. Guidal, M.V. Polyakov, A.V. Radyushkin, M. Vanderhaeghen, Nucleon form-factors from generalized parton distributions, Phys. Rev. D 72 (2005) 054013, arXiv:hep-ph/0410251 [hep-ph].

[32] M. Diehl, P. Kroll, Nucleon form factors, generalized parton distributions and quark angular momentum, Eur. Phys. J. C 73 (4) (2013) 2397, arXiv:1302.4604 [hep-ph].

[33] B. Berthou, D. Binosi, N. Chouika, L. Colaneri, M. Guidal, C. Mezrag, H. Moutarde, J. Rodríguez-Quintero, F. Sabatié, P. Sznajder, et al., PARTONS: PARtonic tomography of nucleon software: a computing framework for the phenomenology of generalized parton distributions, Eur. Phys. J. C 78 (6) (2018) 478, arXiv:1512.06174 [hep-ph].

[34] F. Irani, M. Goharipour, H. Hashamipour, K. Azizi, Impact of recent MINERvA measurement of the antineutrino-proton scattering cross section on the generalized parton distributions, Phys. Rev. D 108 (7) (2023) 074018, arXiv:2306.13060 [hep-ph].

[35] B. Kriesten, P. Velie, E. Yeats, F.Y. Lopez, S. Liuti, Parametrization of quark and gluon generalized parton distributions in a dynamical framework, Phys. Rev. D 105 (5) (2022) 056022, arXiv:2101.01826 [hep-ph].

[36] Y. Guo, X. Ji, K. Shiells, Generalized parton distributions through universal moment parameterization: zero skewness case, J. High Energy Phys. 09 (2022) 215, arXiv:2207.05768 [hep-ph].

[37] Y. Guo, X. Ji, M.G. Santiago, K. Shiells, J. Yang, Generalized parton distributions through universal moment parameterization: non-zero skewness case, J. High Energy Phys. 05 (2023) 150, arXiv:2302.07279 [hep-ph].

[38] G. Duplančić, S. Nabeebaccus, K. Passek-Kumerički, B. Pire, L. Szymanowski, S. Wallon, Probing chiral-even and chiral-odd leading twist quark generalized parton distributions through the exclusive photoproduction of a $\gamma\rho$ pair, Phys. Rev. D 107 (9) (2023) 094023, arXiv:2302.12026 [hep-ph].

[39] S. Kaur, et al., BLFQ, Spatial imaging of proton via leading-twist nonskewed GPDs with basis light-front quantization, Phys. Rev. D 109 (1) (2024) 014015, arXiv:2307.09869 [hep-ph].

[40] M. Constantinou, A. Courtoy, M.A. Ebert, M. Engelhardt, T. Giani, T. Hobbs, T.J. Hou, A. Kusina, K. Kutak, J. Liang, et al., Parton distributions and lattice-QCD calculations: toward 3D structure, Prog. Part. Nucl. Phys. 121 (2021) 103908, arXiv:2006.08636 [hep-ph].

[41] M.J. Riberdy, H. Dutrieux, C. Mezrag, P. Sznajder, Combining lattice QCD and phenomenological inputs on generalised parton distributions at moderate skewness, Eur. Phys. J. C 84 (2) (2024) 201, arXiv:2306.01647 [hep-ph].

[42] G. Duplančić, S. Nabeebaccus, K. Passek-Kumerički, B. Pire, L. Szymanowski, S. Wallon, Accessing chiral-even quark generalised parton distributions in the exclusive photoproduction of a $\gamma\pi^{\pm}$ pair with large invariant mass in both fixed-target and collider experiments, J. High Energy Phys. 03 (2023) 241, arXiv:2212.00655 [hep-ph].

[43] Y. Liu, et al., BLFQ, Skewed generalized parton distributions of proton from basis light-front quantization, Phys. Lett. B 855 (2024) 138809, arXiv:2403.05922 [hep-ph].

[44] X. Luan, Z. Lu, Chiral-odd generalized parton distributions of sea quarks at $\xi = 0$ in the light-cone quark model, Phys. Rev. D 110 (3) (2024) 034021, arXiv:2404.13962 [hep-ph].

[45] S. Bhattacharya, K. Cichy, M. Constantinou, A. Metz, N. Nurminen, F. Steffens, Generalized parton distributions from the pseudodistribution approach on the lattice, Phys. Rev. D 110 (5) (2024) 054502, arXiv:2405.04414 [hep-lat].

[46] N. Arami, F. Taghavi-Shahri, Z.A. Yazdi, S. Shoeibi, F. Arash, The 3D structure of the nucleons in perspective of the GPDs, Int. J. Mod. Phys. A 39 (15n16) (2024) 2450061.

[47] S.V. Goloskokov, Y.P. Xie, X. Chen, Study of gluon GPDs in exclusive $J/\psi$ production in electron-proton scattering, Phys. Rev. D 110 (7) (2024) 076029, arXiv:2408.05800 [hep-ph].

[48] S. Bhattacharya, K. Cichy, M. Constantinou, X. Gao, A. Metz, J. Miller, S. Mukherjee, P. Petreczky, F. Steffens, Y. Zhao, Moments of axial-vector GPD from lattice QCD: quark helicity, orbital angular momentum, and spin-orbit correlation, J. High Energy Phys. 01 (2025) 146, arXiv:2410.03539 [hep-lat].

[49] P. Thakuria, M. Lalung, J.K. Sarma, Exploring twist-3 chiral even generalized parton distributions of light sea quarks in the proton using the light front model, arXiv:2410.20737 [hep-ph].

[50] Z. Ye, J. Arrington, R.J. Hill, G. Lee, Proton and neutron electromagnetic form factors and uncertainties, Phys. Lett. B 777 (2018) 8–15, arXiv:1707.09063 [nucl-ex].

[51] M.E. Christy, T. Gautam, L. Ou, B. Schmookler, Y. Wang, D. Adikaram, Z. Ahmed, H. Albataineh, S.F. Ali, B. Aljawrneh, et al., Form factors and two-photon exchange in high-energy elastic electron-proton scattering, Phys. Rev. Lett. 128 (10) (2022) 102002, arXiv:2103.01842 [nucl-ex].

[52] A. Buckley, J. Ferrando, S. Lloyd, K. Nordström, B. Page, M. Rüfenacht, M. Schönherr, G. Watt, LHAPDF6: parton density access in the LHC precision era, Eur. Phys. J. C 75 (2015) 132, arXiv:1412.7420 [hep-ph].

[53] R.D. Ball, et al., NNPDF, The path to proton structure at 1% accuracy, Eur. Phys. J. C 82 (5) (2022) 428, arXiv:2109.02653 [hep-ph].

[54] S. Navas, et al., Particle Data Group, Review of particle physics, Phys. Rev. D 110 (3) (2024) 030001, https://doi.org/10.1103/PhysRevD.110.030001.

[55] F. James, M. Roos, Minuit: a system for function minimization and analysis of the parameter errors and correlations, Comput. Phys. Commun. 10 (1975) 343–367.

[56] J. Pumplin, D. Stump, R. Brock, D. Casey, J. Huston, J. Kalk, H.L. Lai, W.K. Tung, Uncertainties of predictions from parton distribution functions. 2. The Hessian method, Phys. Rev. D 65 (2001) 014013, arXiv:hep-ph/0101032 [hep-ph].

[57] J. Arrington, W. Melnitchouk, J.A. Tjon, Global analysis of proton elastic form factor data with two-photon exchange corrections, Phys. Rev. C 76 (2007) 035205, arXiv:0707.1861 [nucl-ex].

[58] J.C. Bernauer, et al., A1, Electric and magnetic form factors of the proton, Phys. Rev. C 90 (1) (2014) 015206, arXiv:1307.6227 [nucl-ex].

[59] P.J. Mohr, D.B. Newell, B.N. Taylor, CODATA recommended values of the fundamental physical constants: 2014, Rev. Mod. Phys. 88 (3) (2016) 035009, arXiv:1507.07956 [physics.atom-ph].

[60] E. Tiesinga, P.J. Mohr, D.B. Newell, B.N. Taylor, CODATA recommended values of the fundamental physical constants: 2018*, Rev. Mod. Phys. 93 (2) (2021) 025010.

[61] J.C. Bernauer, et al., A1, High-precision determination of the electric and magnetic form factors of the proton, Phys. Rev. Lett. 105 (2010) 242001, arXiv:1007.5076 [nucl-ex].

[62] X. Zhan, K. Allada, D.S. Armstrong, J. Arrington, W. Bertozzi, W. Boeglin, J.P. Chen, K. Chirapatpimol, S. Choi, E. Chudakov, et al., High-precision measurement of the proton elastic form factor ratio $\mu_p G_E/G_M$ at low $Q^2$, Phys. Lett. B 705 (2011) 59–64, arXiv:1102.0318 [nucl-ex].

[63] M. Mihovilovič, P. Achenbach, T. Beranek, J. Beričič, J.C. Bernauer, R. Böhm, D. Bosnar, M. Cardinali, L. Correa, L. Debenjak, et al., The proton charge radius extracted from the initial-state radiation experiment at MAMI, Eur. Phys. J. A 57 (3) (2021) 107, arXiv:1905.11182 [nucl-ex].

[64] H. Fleurbaey, S. Galtier, S. Thomas, M. Bonnaud, L. Julien, F. Biraben, F. Nez, M. Abgrall, J. Guéna, New measurement of the $1S-3S$ transition frequency of hydrogen: contribution to the proton charge radius puzzle, Phys. Rev. Lett. 120 (18) (2018) 183001, arXiv:1801.08816 [physics.atom-ph].

[65] A. Beyer, L. Maisenbacher, A. Matveev, R. Pohl, K. Khabarova, A. Grinin, T. Lamour, D.C. Yost, T.W. Hänsch, N. Kolachevsky, et al., The Rydberg constant and proton size from atomic hydrogen, Science 358 (6359) (2017) 79–85.

[66] A.D. Brandt, S.F. Cooper, C. Rasor, Z. Burkley, D.C. Yost, A. Matveev, Measurement of the 2S1/2-8D5/2 transition in hydrogen, Phys. Rev. Lett. 128 (2) (2022) 023001, arXiv:2111.08554 [physics.atom-ph].

[67] A. Antognini, F. Nez, K. Schuhmann, F.D. Amaro, Francois Biraben, J.M.R. Cardoso, D.S. Covita, A. Dax, S. Dhawan, M. Diepold, et al., Proton structure from the measurement of $2S-2P$ transition frequencies of muonic hydrogen, Science 339 (2013) 417–420.

[68] Z. Epstein, G. Paz, J. Roy, Model independent extraction of the proton magnetic radius from electron scattering, Phys. Rev. D 90 (7) (2014) 074027, arXiv:1407.5683 [hep-ph].

[69] B. Heacock, T. Fujiie, R.W. Haun, A. Henins, K. Hirota, T. Hosobata, M.G. Huber, M. Kitaguchi, D.A. Pushin, H. Shimizu, et al., Pendellösung interferometry probes the neutron charge radius, lattice dynamics, and fifth forces, Science 373 (6560) (2021) abc2794, arXiv:2103.05428 [nucl-ex].

[70] V.E. Krohn, G.R. Ringo, Reconsiderations of the electron - neutron scattering length as measured by the scattering of thermal neutrons by noble gases, Phys. Rev. D 8 (1973) 1305–1307.

[71] L. Koester, W. Waschkowski, L.V. Mitsyna, G.S. Samosvat, P. Prokofevs, J. Tambergs, Neutrino electron scattering length and electric polarizability of the neutron derived from cross-sections of bismuth and of lead and its isotopes, Phys. Rev. C 51 (1995) 3363–3371.

[72] S. Kopecky, M. Krenn, P. Riehs, S. Steiner, J.A. Harvey, N.W. Hill, M. Pernicka, Neutron charge radius determined from the energy dependence of the neutron transmission of liquid Pb-208 and Bi-209, Phys. Rev. C 56 (1997) 2229–2237.

[73] M.A. Belushkin, H.W. Hammer, U.G. Meissner, Dispersion analysis of the nucleon form-factors including meson continua, Phys. Rev. C 75 (2007) 035202, arXiv:hep-ph/0608337 [hep-ph].

[74] A.A. Filin, D. Möller, V. Baru, E. Epelbaum, H. Krebs, P. Reinert, High-accuracy calculation of the deuteron charge and quadrupole form factors in chiral effective field theory, Phys. Rev. C 103 (2) (2021) 024313, arXiv:2009.08911 [nucl-th].

[75] H. Atac, M. Constantinou, Z.E. Meziani, M. Paolone, N. Sparveris, Measurement of the neutron charge radius and the role of its constituents, Nat. Commun. 12 (1) (2021) 1759, arXiv:2103.10840 [nucl-ex].

[76] K. Borah, R.J. Hill, G. Lee, O. Tomalak, Parametrization and applications of the low-$Q^2$ nucleon vector form factors, Phys. Rev. D 102 (7) (2020) 074012, arXiv:2003.13640 [hep-ph].
[77] Y.H. Lin, H.W. Hammer, U.G. Meißner, New insights into the nucleon's electromagnetic structure, Phys. Rev. Lett. 128 (5) (2022) 052002, arXiv:2109.12961 [hep-ph].
[78] Y.H. Lin, F.K. Guo, U.G. Meißner, The proton charge radius from dimuon photoproduction off the proton, Phys. Lett. B 858 (2024) 139023, arXiv:2407.20375 [hep-ph].
[79] J.J. Chwastowski, K. Piotrzkowski, M. Przybycien, Exclusive lepton pair production at the electron–ion collider, Eur. Phys. J. C 82 (9) (2022) 846, arXiv:2206.02466 [hep-ph].